Ultrasound treatments of tef [*Eragrostis tef* (Zucc.) Trotter] flour rupture starch α-(1,4) bonds and fragment amylose with modification of gelatinization properties

Antonio J. Vela [a], Marina Villanueva [a], Cheng Li [b], Bruce Hamaker [c], Felicidad Ronda [a,*]

[a] *Department of Agriculture and Forestry Engineering, Food Technology, College of Agricultural and Forestry Engineering, University of Valladolid, Valladolid, Spain*
[b] *School of Health Science and Engineering, University of Shanghai for Science and Technology, Shanghai, 200093, China*
[c] *Whistler Center for Carbohydrate Research, Department of Food Science, Purdue University, West Lafayette, IN, USA*

ABSTRACT

Tef is a nutritionally-rich ancient grain gaining increasing interest in gluten-free market. Molecular and structural properties in the main biopolymers of two Spanish ecotypes of tef flour physically modified by ultrasound (US) treatments under different temperatures (20, 40, 45, 50 and 55 °C) were studied. Modifications achieved were dependent on tef ecotype, where white tef presented higher susceptibility. Size-exclusion chromatography indicated higher proportion of intermediate amylose chains (degree of polymerization 300–1600) across the whole amylose chain-length distribution and a higher amylose/amylopectin ratio, that increased up to 23% and 19% in treated samples of white and brown tef respectively. US increased the starch short-range order crystallinity and promoted the formation of random coil protein structure and the disappearance of β-sheet, as confirmed from FTIR spectroscopy. XRD and ^{1}H NMR revealed a higher fragmentation of α-(1,4) than α-(1,6) bonds due ultrasonication. The gelatinization temperature range and ΔH_{gel} decreased after ultrasonication up to 6 °C and 13%, an effect that was reinforced or counteracted, respectively, by the treatment temperature, indicating that annealing modulates the impact of sonication on flour gelatinization properties. Tef starch structural properties were found to be significantly modified by US treatments, where temperature was a determining variable influencing the degree of modification achieved.

1. Introduction

During recent years, the gluten-free (GF) market has grown due to a higher proportion of the population diagnosed with celiac disease, and people who have decided to reduce their gluten consumption for perceived health improvement (Villanueva, Abebe, Collar, & Ronda, 2021). However, removing gluten from products usually leads to diminishment of their quality and represents a technical challenge derived from the structural role that gluten plays. The nutritional profiles of GF products tend to be poorer than traditional products containing gluten, mainly due to the raw materials used, leading to the necessity of diversifying the GF ingredient sources used. Therefore, more attention has been placed on high-nutritional ancient gluten-free grains such as tef. Tef [*Eragrostis tef* (Zucc.) Trotter] is an ancient cereal indigenous to Ethiopia, considered the most important crop in the country. This grain represents a GF source rich in carbohydrate and fiber, having a well-balanced amino acid profile, as well as high content of calcium, copper, iron and zinc, which are higher than those in barley, wheat, and sorghum (Villanueva et al., 2021). Tef grain flours are always whole grain, which further improves the nutritional quality of GF products with additional dietary fiber, starch, protein, and minerals (Bultosa, 2016). In addition, tef has slow-release carbohydrates, which makes it suitable for people with type 2 diabetes and contains a wide variety of bioactive compounds such as phytosterols, vitamins and phenolic compounds, which are closely associated with beneficial effects in human health (Dueñas, Sánchez-Acevedo, Alcalde-Eon, & Escribano-Bailón, 2021). The physicochemical and nutritional quality of tef flours has been shown to be highly dependent on the variety (Abebe, Collar, & Ronda, 2015; Villanueva et al., 2021). Tef varieties are classified in terms of the color of the grains, with white and brown types

being the most common. The identification of tef usually commercialized outside of Ethiopia tends to be attributed to its color and not to the variety of the sample. In Spain, for example, both brown and white tef grains are cultivated and commercialized, but the color does not refer to controlled varieties but to ecotypes obtained from mixtures of different varieties of the same color. The testa, located within the pericarp, is filled with pigmented material such as tannins or polyphenolic compounds, giving a darker color associated with a thicker testa (Abebe et al., 2015).

The natural properties of GF raw materials limit the application where they can be used (Acevedo, Villanueva, Chaves, Avanza, & Ronda, 2022). In the food industry, physical modifications have been applied to flours and starches to improve their properties and expand their range of utilization. Ultrasound (US) treatments is a feasible technique to generate such physical modifications. The term ultrasound refers to sound waves that exceed the audible threshold of human hearing (18 kHz) and create high-energy vibrations (Amini, Razavi, & Mortazavi, 2015). The modification that US generate in flours and starches depend greatly on treatment factors such as sonication power and frequency, time and temperature of the treatment, and on properties of the treated suspension such as concentration, botanical origin of the studied matter, and the solvent's capacity for absorbing and transmitting US energy (Amini et al., 2015; Vela, Villanueva, Solaesa, & Ronda, 2021). Sinusoidal ultrasound waves passing through the aqueous medium generate pressure variation within the liquid that induces mixing of the suspension. During the expansion cycle tiny bubbles are formed from the existing gas in the fluid, which shrink during the compression cycle. Over numerous cycles, the bubbles keep growing to the point that the oscillation of their wall equals that of the applied frequency and implodes during one compression cycle, known as the cavitation phenomenon (Zhu, 2015). The continuous collapse of the tiny bubbles generates micro-jets that impact the treated particles and induce granular and molecular damage (Yang et al., 2019). The sonication process results in an inherent temperature increase in the treated suspension as consequence of heating derived from cavitation. Furthermore, in excess of water (>60%) (as occurs in sonication) and temperatures below gelatinization conditions, flours and starches undergo annealing processes, which leads to changes in their physicochemical properties that are dependent on the suspension temperature (Zavareze & Dias, 2011). If temperature is not controlled during US treatment, it does not remain stable and may even lead to starch gelatinization. Hence, temperature at which the US treatment is carried out is an important subject of study in determining its influence in the extent of modification achieved by ultrasonication.

The effect of US on techno-functional and rheological properties of rice flour has been previously studied in depth (Vela, Villanueva, & Ronda, 2021; Vela, Villanueva, Solaesa, & Ronda, 2021). However, neither starches nor refined flours could predict the effect that US treatments would have in a whole grain flour with a much more complex composition such as tef. All components present in a whole grain flour (i. e., starch, proteins, fiber, fat, and minerals) are vulnerable to be affected by US cavitation to different degrees depending on their susceptibility. The novelty proposed by the present study was to determine the degree of modification caused to the molecular and structural characteristics of two ecotypes of tef flour (white and brown) by ultrasound treatments depending on the applied treatment temperature (in the range of 20 °C–55 °C) and the impact on their gelatinization and retrogradation properties. Starch fine molecular structures are of essential importance in determining its techno-functional and pasting properties (Li, Hu, Huang, Gong, & Yu, 2020), therefore, gaining deeper understanding at a structural level will allow setting the correlation between ultrasonication conditions and molecular structure that leads to obtaining an optimum flour functionality and an adequate.

2. Materials and methods

2.1. Tef flours

The grains of tef of the two Spanish ecotypes studied, white and brown, grown under the same conditions, were supplied by CYLTEF (CYLTEF, Villanazar, Spain). Tef grains were milled in a LM3100 hammer mill (Perten Instruments, Stockholm, Sweden) with 0.5 mm opening screen size to obtain the whole flour of both tef samples. The proximal composition of the white (WT) and brown (BT) tef flours was: 10.2% and 9.0% protein, 6.7% and 7.0% fiber, 2.2% and 2.6% lipids, 65.4% and 67.1% starch and 10.9% and 8.9% moisture, respectively. Total protein content (N x 5.7) was analyzed by the titrimetric method using a Kjeldahl distillation unit following AOAC method 960.52–1961 (2010). Dietary fiber was analyzed by the AOAC method 991.43 (1994). Lipids content was determined by the gravimetric method using a Soxhlet apparatus with hexane as the extraction solvent according to the AOAC method 923.05–1923 (1996). Starch content was determined by the amylose/amylopectin assay kit (Megazyme, Wicklow, Ireland). The average moisture content was measured following the Official AACC Method 44–19 (AACC, 1999). All the assays were conducted in duplicate.

2.2. Ultrasound treatment

Tef flour dispersions were prepared at a concentration of 25% (g dry flour/100g of dispersion) in distilled water (total weight of 400 g). Ultrasound treatment consisted of 10 min sonication at a constant frequency of 24 kHz with a maximum outlet power of 180 W and 80% on-off pulse, using a Hielscher UP400St sonicator (Hielscher Ultrasonics, Teltow, Germany) paired with a S24d22D titanium tip. This time was chosen given that a previous study performed on rice flour showed that 10 min was enough to achieve similar modification effect as longer treatments (i.e., 40 and 60 min) (Vela, Villanueva, Solaesa, & Ronda, 2021). Dispersions were stirred during treatment using a magnetic stirrer to ensure homogenous temperature and avoid flour sedimentation. The treatment temperatures were set below the native flours' onset gelatinization temperature (62.42 ± 0.09 °C for white tef and 64.80 ± 0.04 °C for brown tef), at 20, 40, 45, 50, and 55 °C (refer to Table 1) and were kept constant during treatment using recirculating water from a LAUDA RA12 water bath (LAUDA, Lauda-Königshofen, Germany). After treatment, suspensions were freeze-dried using a Telstar Lyoquest equipment (Telstar, Terrassa, Spain), and later sieved to < 250 μm. Untreated native flours were used as the control in the study. All flours were stored at 4 °C until use.

2.3. Scanning electron microscopy (SEM)

A Quanta 200FEG scanning electron microscope (ELECMI, Zaragoza, Spain) equipped with X-ray detector was used to obtain images of the samples' microstructure. Samples were evaluated in low vacuum mode without prior metallization, with an accelerating voltage of 5 keV using a secondary electron detector at magnifications of 100 ×, 500 ×, 1500 × and 3000 ×.

Table 1
Sample identification for the studied flours.

White Tef	Brown Tef	Ultrasonication	Treatment temperature (°C)
WT-C	BT-C	No	–
WT-20	BT-20	Yes	20
WT-40	BT-40	Yes	40
WT-45	BT-45	Yes	45
WT-50	BT-50	Yes	50
WT-55	BT-55	Yes	55

WT: White tef. BT: Brown tef. C: Control.

2.4. X-ray diffraction (XRD)

XRD patterns of the flours were recorded using a Bruker-D8-Discover-A25 diffractometer (Bruker, Billerica, MA, USA) coupled with Cu-Kα radiation (λ = 0.154 nm) at a voltage of 40 kV and current of 40 mA. Radiation intensities were recorded from 5° to 40° at 2θ diffraction angle, with a scan step size of 0.02°, receiving slit width of 0.02 nm, scatter slit width of 2.92°, divergence slit width of 1°, and a rate of 1.2°/min. Samples were previously equilibrated at 15% humidity using a saturated humidity ICP260 incubator at 15 °C (Memmert GmbH, Schwabach, Germany). Samples' crystallinity was calculated as described by Vela, Villanueva, Solaesa, and Ronda (2021).

2.5. Size-exclusion chromatography (SEC)

The chain-length distribution of debranched starches was analyzed in duplicate with an Agilent 1260 size exclusion chromatography (SEC) system (Agilent Technologies, Santa Clara, CA, USA) equipped with an Optilab refractive index detector (RID) (Wyatt Technology, Santa Barbara, CA, USA). A set consisting of a GRAM pre-column, GRAM 100 and GRAM 1000 analytical columns (PSS GmbH, Mainz, Germany) connected in series was used for the analysis. The mobile phase consisted of DMSO containing 0.5% (w/w) LiBr (DMSO/LiBr solution) at a flow rate of 0.6 mL/min and 70 °C, following a previously described method (Cave, Seabrook, Gidley, & Gilbert, 2009; Martinez et al., 2018). Starch was isolated from tef flours (native and ultrasonicated) following the procedure indicated by Martinez et al. (2018). The debranching reaction was carried out with isoamylase (Megazyme, Wicklow, Ireland) at 37 °C for 3 h. Pullulan standards (PSS GmbH, Mainz, Germany) with molecular weights ranging from 342 to 6.36×10^5 were used for calibration, allowing to convert elution volume to hydrodynamic volume (V_h) following the Mark-Houwink equation with the parameters K = 2.424 × 10^{-4} dL/g and α = 0.68 (Cave et al., 2009). V_h was converted to the degree of polymerization (DP) using the Mark-Houwink equation (Vilaplana & Gilbert, 2010). The SEC weight distributions, w(logV_h), were obtained from the RID signal and plotted as a function of DP. Amylose (AM) content was inferred from dividing the area under the curve (AUC) of the amylose peak (DP ≥ 100) by the total area under the curve of both amylopectin (AP) and amylose peaks (Martinez et al., 2018). All samples were normalized to yield the same AUC for better comparing changes among treatments. Amylopectin chains were divided as short (AP1) and long branches (AP2), corresponding to DP around 10 and 30, respectively. The amylose chain-length distributions (CLD) were divided into three DP regions, representing short (AM1: DP ~100–300), medium (AM2: DP ~ 300–1600) and long chains (AM3: DP > 1600) (Wang et al., 2015). Samples were fitted to individual peaks following iterative fitting assuming Gaussian band shapes using Origin2019b (OriginLab Corporation, Northampton, MA, USA) for better quantitative comparison of the structural differences. The amount corresponding to each region was determined as the AUC of the region divided by the total AUC of the three regions.

2.6. Fourier transform infrared (FTIR) spectroscopy

FTIR spectra of the flours were obtained using a FT-IR Nicolet iS50 spectrophotometer (Thermo Fisher Scientific, Waltham, MA, USA) equipped with a crystal diamond attenuated total reflectance (ATR) sampling accessory. Samples were equilibrated at 15% humidity prior measurement (see Section 2.4). The scanning was made in the range of 4000-400 cm^{-1} with resolution of 4 cm^{-1} and accumulation of 64 scans. Protein changes were analyzed in amide I bands (1700-1600 cm^{-1}) using Origin2019b (OriginLab Corporation, Northampton, MA, USA), by determination of individual bands with second derivative analysis following iterative fitting assuming Gaussian band shapes. Peak assignment corresponds to: β-turns (1700-1660 cm^{-1}), α-helix (1658-1650 cm^{-1}), random coil (1650-1640 cm^{-1}) and β-sheet (1640-1600

cm^{-1}). Samples were measured in duplicate.

2.7. Proton nuclear magnetic resonance (^{1}H NMR) spectroscopy

^{1}H NMR analyses were performed using a 500 MHz NMR spectrometer (Agilent Technologies, Santa Clara, CA, USA) coupled with OneNMR probe at 70 °C, 45° pulse width, spectral width of 8012.8 Hz, a total of 400 transients, acquisition time of 2.004 s and a relaxation delay of 5 s, as indicated by Acevedo et al. (2022). Each sample (~7 mg) was placed into a vial with 600 μL of deuterated DMSO, 50 μL of deuterated trifluoroacetic acid (TFA-d) and 3 mg LiBr, and transferred to an NMR tube. Spectra were analyzed using MestReNova software v.12 (Mestrelab Research Co., Santiago de Compostela, Spain). The starch degree of branching (DB) was determined from the results of ^{1}H NMR following the equation:

$$DB = \frac{I_{\alpha-(1,6)}}{I_{\alpha-(1,6)} + I_{\alpha-(1,4)}} * 100\%$$

Where $I_{\alpha-(1,6)}$ is the AUC of the peak corresponding to α-(1,6)-glucosidic bonds at ~4.80 ppm and $I_{\alpha-(1,4)}$ is the AUC of the peak corresponding to α-(1,4)-glucosidic bonds at ~5.12 ppm. Each sample was measured in duplicate.

2.8. Thermal properties

Gelatinization and retrogradation transitions were analyzed by differential scanning calorimetry (DSC) (Mettler Toledo, Barcelona, Spain). Flour samples (~6 mg) were weighed into 40 μL aluminum pans and distilled water was added to reach a flour:water ratio of 30:70 (w/w). The pans containing the samples were kept at room temperature for 30 min for moisture equilibration prior measurement. The scan consisted of heating from 0 to 110 °C at 5 °C/min using an empty sealed pan as reference. Onset (T_O), peak (T_P) and conclusion (T_C) temperatures (°C) and enthalpy change (ΔH, J/g of dry matter, dm) of endothermic transitions were recorded. The first scan was used to study the gelatinization transition, and a second run performed after 7 days of sample storage at 4 °C to assess degree of retrogradation. The dissociation of the amylose-lipid complex was also studied in both runs. Each sample was measured in duplicate.

2.9. Statistical analysis

Results were statistically analyzed using Statgraphics Centurion XVIII software (Statgraphics Technologies Inc., The Plains, VA, USA). Analysis of variance (ANOVA) by Least Significant Difference (LSD) test at p-value ≤0.05 was performed.

3. Results and discussion

3.1. Morphology

Scanning electron micrographs of selected samples are shown in Fig. 1. Native flours (Fig. 1A and 1D) present compact structures of starch granules packed together attached to protein (Abebe et al., 2015). Sonicated samples present clear signs of surface disruption in these structures. The 100 × magnifications of the treated samples (B1, C1, E1 and F1) reveal the presence of particles of smaller size which seem to be small groups of starch granules that were released from the packed structure. The highest magnification (500 ×) allows the visualization of how the shape of the original packed structure has changed, resulting in a much more fragmented structure. These differences are a consequence of the cavitation phenomenon, since the collapsing bubbles generate material fatigue and gradual tearing off of microscopic particles, leading to surface damage (Degrois, Gallant, Baldo, & Guilbot, 1974). The 1500 × and 3000 × magnifications show that, in treated samples, there are

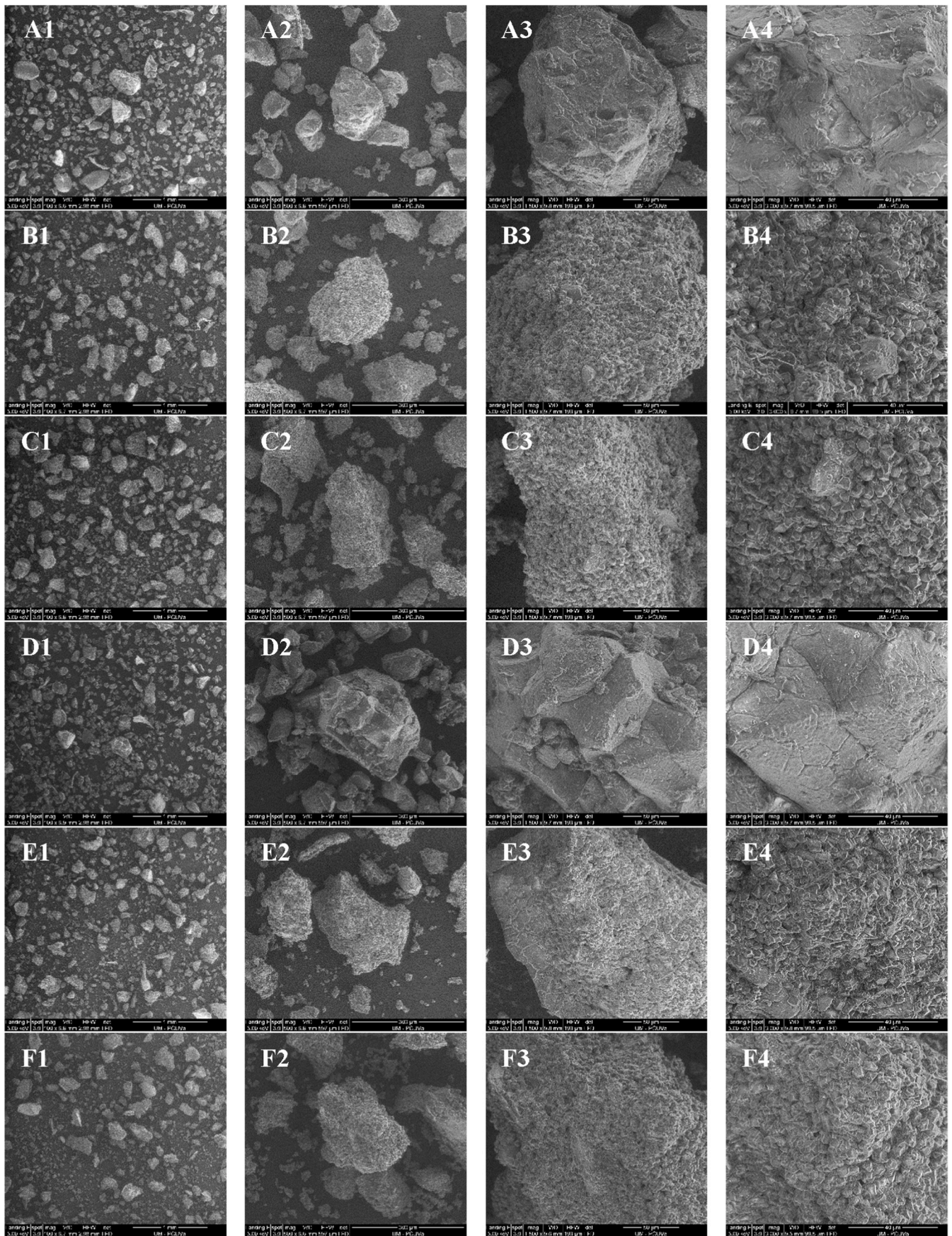**Fig. 1.** SEM images of (A) WT-C, (B) WT-20, (C) WT-55, (D) BT-C, (E) BT-20 and (F) BT-55 at a magnification of (1) 100 $\times$, (2) 500 $\times$, (3) 1500 $\times$ and (4) 3000 $\times$.

loosened starch granules with more exposed area, giving a more rugged appearance to the surface in comparison to the native flours. Similar structural damage has been reported before for ultrasound treated samples (Acevedo et al., 2022; Amini et al., 2015; Vela, Villanueva, & Ronda, 2021; Vela, Villanueva, Solaesa, & Ronda, 2021). Few physical differences were observed between samples treated at 20 °C (Fig. 1B and E) and 55 °C (Fig. 1C and F). It is believed that the determined impact depends greatly on US and not so much in the treatment temperature, especially in short time treatments. The tef ecotype did not visibly affect the impact of the treatments.

3.2. X-ray diffraction (XRD)

The X-ray diffraction patterns and their calculated crystallinity are presented in Fig. 2. All spectra showed the A-type crystalline pattern for cereals, with five characteristic peaks at scattering angles (2θ) of 15, 17, 18, 23 and 26°, and the reflection at 20°, associated to V-crystallinity (Villanueva, Harasym, Muñoz, & Ronda, 2018). The diffraction patterns and their intensities after treatments hardly differed from the corresponding control flour. The determined long-range order crystallinity remained unchanged for both tef ecotypes at lower treatment temperatures, but it was significantly increased when white tef was treated at higher temperatures (>40 °C). In brown tef, the same tendency was determined, but no significant differences were obtained. The observed trend is similar to the increased crystallinity reported after US treatments of rice flour at increasing temperature (Vela, Villanueva, & Ronda, 2021). Ultrasonication has been reported to cause small changes in starch and flour crystallinity content (Amini et al., 2015; Vela, Villanueva, Solaesa, & Ronda, 2021), believed to be because US preferentially degrades amorphous domains, while crystalline regions are more resistant and remain mostly unaffected (Luo et al., 2008). Higher temperatures during US treatment, where the flour is kept in excess water, could lead to an improved starch crystallinity by facilitating interactions between the starch chains (Zavareze & Dias, 2011), due to a more compact structure after reorganization of starch molecules and higher content of amylopectin double helices in those ultrasonicated samples. It seems that an apparent increased crystallinity could result from better packed starch structure due to the effect of US (higher amount of shorter amylose chains) and the treatment temperature (enhanced mobility of amorphous regions).

3.3. Chain-length distribution (CLD) of debranched starch

Size-exclusion chromatography was used to evaluate the distribution of chain lengths and to quantify structural changes in starch caused by ultrasound treatments, since it allows the characterization of amylose chains and amylopectin branches (Li et al., 2020). The SEC weight CLDs obtained from debranched samples are shown in Fig. 3, and the structural parameters are presented in Table 2. All samples showed the

typical bimodal distribution for amylopectin branches (DP < 100), with maximum values at DP ~ 10 and DP ~ 30 representing short (AP1) and long (AP2) amylopectin chains, respectively, and a broad peak for amylose (AM) (DP ≥ 100) linear chains (Li et al., 2020; Martinez et al., 2018; Wang et al., 2015). Given that the intensity of the RID signal is proportional to the mass concentration of the sample, all distributions have been normalized to yield the same total area under the curve (AUC) to facilitate comparison among samples and compare proportional changes among amylose and amylopectin. The length of short and long amylopectin branches is denoted as X_{AP1} and X_{AP2}, respectively, and the molar ratio of long to short amylopectin chains is represented as h_{AP2}/h_{AP1}. Results showed few differences among the determined values of X_{AP1} and X_{AP2}, meaning that the modal length of short and long amylopectin branches was not significantly affected by US treatments. The height of these peaks, however, was lower in treated samples after being normalized to yield the same AUC (see Fig. 3), indicative of lower relative presence of amylopectin branches after ultrasonication. The ratio h_{Ap2}/h_{Ap1} remained unaltered for BT treatments, but for WT a significant increase was observed for treatments at 45, 50 and 55 °C, due to lower proportion of h_{AP1} in the AP chains. It has been previously indicated that the main degradation of starches at short treatment times is caused to the amorphous regions (Amini et al., 2015; Luo et al., 2008), but as time increases, the waves are prompted to also attack the inner lamellae which are more crystalline and richer in amylopectin chains (Flores-Silva et al., 2017). The fragments of amylopectin generated by the physical damage caused by US to starch are solubilized and are not quantified by SEC analyses (Han, Campanella, Mix, & Hamaker, 2002). It is believed that these fragmented amylopectin chains remained as crystallites since their presence is still detected when the modified flours are analyzed in a solid state, as was seen in XRD (see Fig. 2).

Amylose (AM) ratio, estimated as the AUC of amylose peak (DP ≥ 100) divided by the total AUC of both amylopectin and amylose peaks, was increased after ultrasonication in all studied temperature treatments believed to be consequence of the lost fraction of soluble short amylopectin chains, which increased the proportion of amylose in the ultrasonicated samples (see Table 2). AM ratio varied depending on the botanical origin, though the trend of the effect that US treatments at different temperature had on them was similar. Treated WT samples did not show significant differences among them, while in BT the determined values for samples treated at 45, 50 and 55 °C were significantly lower than samples sonicated at 20 and 40 °C. Amylose weight CLDs had three overlapping peaks (Wang et al., 2015), which were divided in three different groups, AM1, AM2 and AM3, corresponding to short (DP ~ 100–300), intermediate (DP ~ 300–1600) and long (DP > 1600) amylose chains, respectively. These groups were fitted to individual peaks to facilitate quantitative comparison (fits are shown in Supplementary Fig. 1 and Supplementary Fig. 2). The percentage of each group peak area was calculated as the ratio to the total AM AUC to indicate the proportion of chains in each group. Long amylose chains were mainly affected by US treatments, resulting in a significant reduction of long amylose chains (AUC$_{AM3}$) in sonicated samples, while increasing the amount of intermediate amylose chains (AUC$_{AM2}$). Partial depolymerization of amylose has been reported in ultrasonication of starches, resulting in increased amount of shorter linear fragments (Babu, Mohan, & Parimalavalli, 2019; Karwasra, Kaur, & Gill, 2020). Czechowska-Biskup, Rokita, Lotfy, Ulanski, and Rosiak (2005) showed that US causes polymer fragmentation in a non-random manner and that there is a definite chain length limiting the degradation process, which in the case of tef flours seems to be among long amylose chains (Czechowska-Biskup et al., 2005). The proportion of shorter chains (AUC$_{AM1}$) was also reduced, related to the higher presence of AUC$_{AM2}$. In agreement, the peak maximum of amylose chains (X_{AM}) was significantly increased in treated samples with respect to their corresponding control flour, meaning that the presence of intermediate chains was higher after US treatments, displacing the peak maximum towards higher DP. The chain fragmentation determined by SEC analysis suggests that α-(1,4) glycosidic bonds from amylose and amylopectin
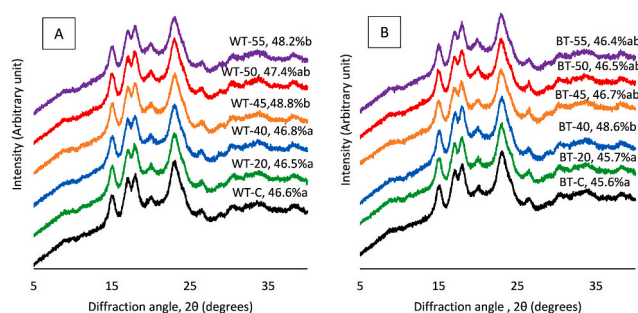

Fig. 2. XRD pattern of the (A) white tef and (B) brown tef studied samples. The crystallinity degree of each sample is indicated on the curve. (For interpretation of the references to color in this figure legend, the reader is referred to the Web version of this article.)
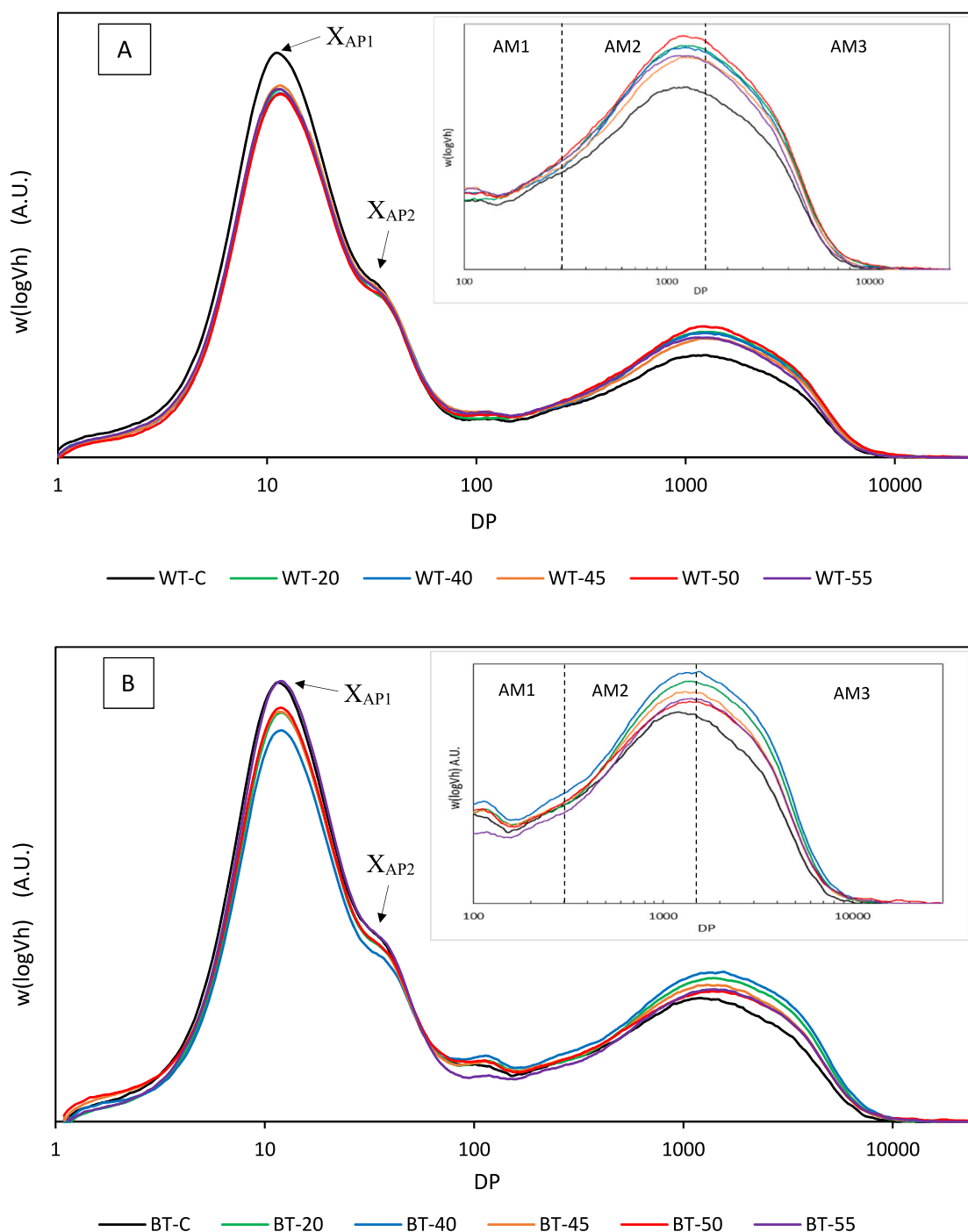
Fig. 3. Size exclusion chromatograms of debranched white (A) and brown (B) starch samples, with enlargement of the amylose regions as function of DP. (For interpretation of the references to color in this figure legend, the reader is referred to the Web version of this article.)

suffered greater rupture by sonication than the degradation caused to α-(1,6) glycosidic bonds, as will be shown in section 3.5.

3.4. Fourier transform infrared (FTIR) spectroscopy

FTIR spectra were used to evaluate molecular changes in the short-range/double helical order of starch (1200-900 cm^{-1}) and in the secondary structure of proteins (the amide I region, 1700-1600 cm^{-1}) (see data in Table 3). For starch analysis, the band intensities at 1045, 1022 and 995 cm^{-1} are related to the crystalline regions, amorphous regions

and bonds in the hydrated helices of carbohydrates (C–OH bending vibrations), respectively (Yong et al., 2018). The band intensity ratio 1047/1022 is used to quantify the degree of short-range order in starch, and 1022/995 indicates the proportion of amorphous to ordered structure of starch (Yong et al., 2018). Treated samples showed decreased values of the 1047/1022 and 1022/995 ratios, without being influenced by the applied temperature. The decreased 1047/1022 ratio indicates impact of US on the crystalline regions, resulting from chain degradation and favoring the proportion of amorphous regions in treated starch granules, which is in agreement with the higher presence of

Table 2
Structural parameters of the tef samples determined by SEC.

Sample	X_{AP1}	X_{AP2}	X_{AM}	h_{AP2}/h_{AP1}	AM ratio (%)	AUC_{AM1} (%)	AUC_{AM2} (%)	AUC_{AM3} (%)
WT-C	11.2a	32.7a	996a	0.442 ab	30.0a	23.3b	49a	27.4b
WT-20	11.5a	33.5a	1087b	0.438a	34.5b	20.7a	67b	12.8a
WT-40	11.4a	33.0a	1121b	0.458bc	34.2b	19.7a	68b	12.6a
WT-45	11.5a	31.6a	1116b	0.464c	33.7b	19.7a	66b	14.8a
WT-50	11.5a	32.5a	1091b	0.462c	34.9b	19.7a	66b	13.8a
WT-55	11.5a	31.0a	1081b	0.471c	33.5b	19.5a	67b	13.5a
SE	0.1	0.8	18	0.005	0.7	0.5	1	0.8
Analysis of variance and significance (p-values)								
	ns	ns	*	*	*	*	***	***
BT-C	11.5a	33.9bc	1090a	0.436a	31.9a	20.8a	51.6a	27.5c
BT-20	11.7a	32.2a	1170bc	0.446a	35.8c	19.5a	67.2cd	13.3a
BT-40	11.7a	33.9bc	1180c	0.437a	37.0d	19.1a	66.3c	14.6 ab
BT-45	11.7a	32.2a	1114 ab	0.451a	34.9bc	19.4a	66.0c	14.6 ab
BT-50	11.8a	34.1c	1118 ab	0.439a	34.1bc	18.3a	68.4d	13.4a
BT-55	11.8a	32.7 ab	1150abc	0.444a	33.4 ab	21.0a	62.6b	16.4b
SE	0.2	0.4	18	0.007	0.5	0.8	0.6	0.8
Analysis of variance and significance (p-values)								
	ns	*	ns	**	ns	ns	***	***

X_{AP1}, X_{AP2}: DP of peak maximum of short and long amylopectin chains, respectively. X_{AM}: DP of peak maximum of amylose chains. h_{AP2}/h_{AP1}: height ratio of AP2 to AP1. AM ratio: area under the curve of amylose peak divided by the total area under the curve of amylopectin and amylose peaks. AUC_{AM1}, AUC_{AM2}, AUC_{AM3}: Percentual area under the amylose peak corresponding to short, intermediate, and long amylose chains, respectively.
SE: Pooled standard error from ANOVA. Different letters in the same column within each studied variety indicate statistically significant differences between means at $p < 0.05$.
Analysis of variance and significance: ***$p < 0.001$. **$p < 0.01$. *$p < 0.05$. ns: not significant.

Table 3
Starch bands analysis and secondary structure content of the studied flours.

	Starch bands		Protein secondary structure analysis (%)			
Sample	IR 1047/ 1022	IR 1022/ 995	α-Helix	β-Sheet	β-Turn	Random coil
WT-C	0.805b	0.910b	38 ab	21.9d	10 ab	30a
WT-20	0.701a	0.824a	35 ab	12.8a	9a	43b
WT-40	0.705a	0.839a	39 ab	14.3a	9a	38 ab
WT-45	0.712a	0.833a	33a	16.2bc	13b	37 ab
WT-50	0.697a	0.826a	39 ab	18.7c	11 ab	31a
WT-55	0.689a	0.809a	40b	17.9c	9a	34a
SE	0.008	0.01	2	0.8	1	2
Analysis of variance and significance (p-values)						
	***	*	ns	**	ns	*
BT-C	0.790b	0.905b	37 ab	17.8b	6.4a	38 ab
BT-20	0.714a	0.842a	34 ab	13.8a	10.6bc	41b
BT-40	0.693a	0.830a	36 ab	16.2 ab	7.5a	40 ab
BT-45	0.698a	0.841a	38b	16.4 ab	9.1 ab	36 ab
BT-50	0.694a	0.840a	35 ab	17.7b	10.9bc	36 ab
BT-55	0.694a	0.830a	32a	19.9b	12.6c	35a
SE	0.009	0.01	2	0.9	0.9	2
Analysis of variance and significance (p-values)						
	**	*	ns	ns	*	ns

SE: Pooled standard error from ANOVA. Different letters in the same column within each studied variety indicate statistically significant differences between means at $p < 0.05$.
Analysis of variance and significance: ***$p < 0.001$. **$p < 0.01$. *$p < 0.05$. ns: not significant.

intermediate amylose chains determined with SEC for US treated flours. Similar results have been found in ultrasound treated rice flour at different temperatures (Vela, Villanueva, & Ronda, 2021). In the case of the 1022/995 ratio, the obtained decreases refer to higher proportion of double helices in starch granules, meaning that US treatments led to an improved ordered structure within the starch granule, probably due to the high moisture content and moderate thermal energy during treatment, which allow chain mobility for a better packed structure (Zavareze & Dias, 2011).

The secondary structure of proteins was analyzed by Gaussian curve-fitting of amide I band. Four individual peaks were determined: β-turns (1700-1660 cm^{-1}), α-helix (1658-1650 cm^{-1}), random coil (1650-1640 cm^{-1}) and β-sheet (1640-1600 cm^{-1}) (see Supplementary Figs. 3 and 4). The relative area of each individual peak was used to compare changes in the secondary structure of proteins derived from treatment conditions. In the case of white tef (WT), the control sample had the highest proportion of β-sheet (21.9%) and the lowest content of random coil (30%), while in ultrasonicated WT flours the amount of β-sheet was reduced [up to 12.8% (WT-20)] and random coil was increased [up to 43% (WT-20)]. Similar results were obtained by Vela, Villanueva, and Ronda (2021) in the secondary structure of rice flour proteins. Results showed more marked change for the lower temperature treatments, indicating that this effect was mainly caused by US cavitation and that it was attenuated by increasing temperature. α-Helix and β-turns were not significantly altered by treatments. The treated brown tef (BT) samples showed few differences with respect to the control sample; unaltered contents of α-helix, β-sheet and random coil were determined, while β-turn was increased. XRD and analysis of amylopectin branches by SEC also indicated a slightly higher effect of treatment on white tef than brown tef, suggesting that BT flours may have a more resistant structure.

3.5. Nuclear magnetic resonance (NMR) spectroscopy

The resonance of anomeric protons involved in α-(1,4) and α-(1,6) glycosidic bonds were analyzed using ^{1}H NMR spectroscopy to evaluate structural features of the studied flours. ^{1}H NMR is a powerful and reliable technique to determine the degree of branching (DB) of starches (Xu, Chen, Luo, & Lu, 2019). The obtained spectra and their DB (%) are presented in Fig. 4. The anomeric signals α-(1,4) and α-(1,6) appeared at 5.12 and 4.80 ppm, respectively, in agreement with those reported for other starches (Acevedo et al., 2022; Xu et al., 2019). Both tef ecotypes showed a slight increase of DB after treatments. WT samples followed a decreasing trend with increasing treatment temperature, while BT samples did not show any trend. The highest studied temperature showed the closer value to the control sample (5.19% and 5.02% in WT; 4.36% and 4.24% in BT), in concordance with the minimum amylose increase obtained in SEC analyses, indicating that increasing
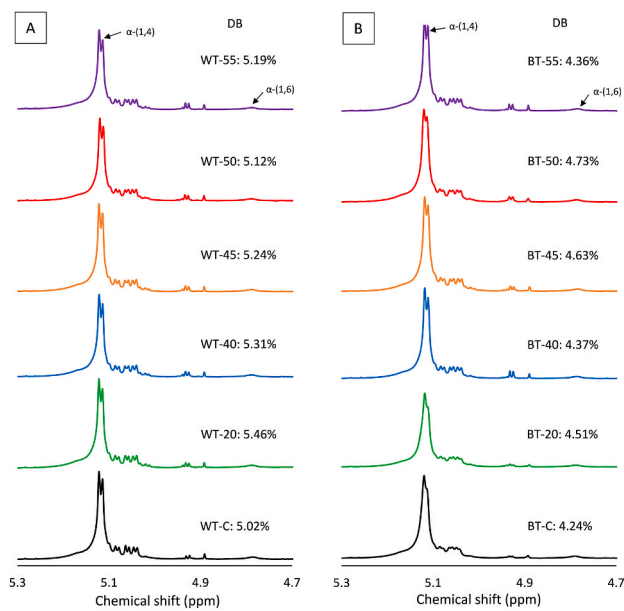
Fig. 4. ^{1}H NMR spectra and degree of branching (DB) of the studied white (A) and brown (B) tef flours. (For interpretation of the references to color in this figure legend, the reader is referred to the Web version of this article.)

temperature and annealing phenomenon counteract the effect of cavitation. These results suggest greater rupture of α-(1,4) glycosidic bonds from amylose and amylopectin and slower degradation of α-(1,6) glycosidic bonds from amylopectin, in agreement with the preferential amylose degradation determined by XRD, SEC and FTIR. A marked decreased degree of branching has been reported by Acevedo et al. (2022) after ultrasonication of cowpea starch. These differences are believed to derive from the applied sonication time, given that in that study the sonication time was much longer (30 min) than the time

applied in the current study (10 min). Others have shown that in short US exposure times the amorphous regions are mainly degraded while amylopectin chains are more resistant (Luo et al., 2008).

3.6. Thermal properties

The thermal properties of native and treated flours are presented in Table 4. These properties provide information about the gelatinization and retrogradation transitions of starch, of high relevance on its industrial applicability as raw ingredients in starch-containing food formulation. Two endotherms were observed during the first scan (see Supplementary Fig. 5), the first one attributed to starch gelatinization and the later peak attributed to melting of amylose-lipid complexes (Klucinec & Thompson, 1999). The range between the onset and conclusion temperatures of gelatinization peak [ΔT ($T_{C\text{-gel}} - T_{O\text{-gel}}$)] represent the homogeneity degree of crystallites, while ΔH_{gel} reflects the energy needed to disrupt the molecular order associated with the crystallinity (Wang et al., 2015). The narrowing of ΔT in all treatments was mainly caused by modification of $T_{C\text{-gel}}$ rather than $T_{O\text{-gel}}$, confirmed as an effect of US cavitation potentiated by annealing. $T_{O\text{-gel}}$ and $T_{C\text{-gel}}$ are related to the melting temperatures of the weakest and strongest crystallites in starch, respectively (Wang, Wang, Zhou, Wu, & Ouyang, 2022). $T_{O\text{-gel}}$ was not modified by ultrasonication when applied at temperatures ≤50 °C but was significantly increased at 55 °C as consequence of annealing. It is believed that higher temperatures promoted rearrangement of the weakest crystallites in starch structure by improving mobility of chains, resulting in higher interactions between amylose-amylose and/or amylose-amylopectin chain, more susceptibility to double helices formation, and greater order that requires higher temperature to be disrupted (Zavareze & Dias, 2011). Results showed that ultrasonication caused a significant decrease of the conclusion temperature ($T_{C\text{-gel}}$), indicative that cavitation disrupted the most ordered double-helical structures and reduced the amount and stability of the better packed crystallites, thus lowering the dissociation temperature (Wang, Xu, et al., 2020; Wang, Wu, et al., 2020). Starches with longer amylopectin branch chains and higher crystallinity display

Table 4
Thermal properties of the studied flours.

Sample	First scan							Second scan					
	ΔH_{gel} (J/g)	$T_{O\text{-gel}}$ (°C)	$T_{P\text{-gel}}$ (°C)	$T_{C\text{-gel}}$ (°C)	ΔT (°C)	$\Delta H_{am\text{-lip}}$ (J/g)	$T_{O\text{-am-lip}}$ (°C)	ΔH_{ret} (J/g)	$T_{O\text{-ret}}$ (°C)	$T_{P\text{-ret}}$ (°C)	$T_{C\text{-ret}}$ (°C)	$\Delta H_{am\text{-lip-ret}}$ (J/g)	$T_{O\text{-am-lip-ret}}$ (°C)
WT-C	9.0bc	62.4a	69.1a	76.6b	14.2d	0.5a	87a	3.4a	36.1a	51.3a	62.4b	1.05bc	84.7a
WT-20	7.8a	62.3a	68.6a	75.8a	13.5c	0.5a	87a	3.9bc	36.1a	50.3a	62.4b	1.14c	87.2cd
WT-40	8.3 ab	62.3a	68.6a	75.3a	13.0b	0.7a	86a	4.1c	36.9a	50.3a	63.0b	0.84a	88.2d
WT-45	8.5 ab	62.3a	68.8a	75.5a	13.2bc	0.7a	86a	3.9bc	36.5a	51.0a	62.9b	0.87a	88.3d
WT-50	8.6 ab	62.2a	68.6a	75.3a	13.1bc	0.6a	88a	3.7b	39.4b	50.3a	62.5b	0.91 ab	86.1bc
WT-55	9.4c	63.5b	68.7a	75.2a	11.7a	0.7a	87a	3.8b	38.4b	50.1a	61.7a	1.09c	85.5 ab
SE	0.2	0.1	0.2	0.2	0.1	0.1	1	0.1	0.4	0.6	0.2	0.04	0.4
Analysis of variance and significance (p-values)													
	*	***	ns	*	***	ns	ns	*	**	ns	*	*	**
BT-C	8.6b	64.8a	71.1a	78.8c	14.0c	0.5a	90b	4.1 ab	37.6a	50.9a	62.9a	1.6c	84.2a
BT-20	8.0a	64.4a	70.7a	77.4b	13.0b	0.6 ab	89 ab	4.3b	37.3a	50.6a	63.3a	0.9 ab	85.7abc
BT-40	8.1a	64.7a	70.9a	77.8b	13.1b	0.7b	87a	3.9 ab	38.1a	50.3a	62.3a	1.2abc	87.1bc
BT-45	7.9a	64.7a	71.0a	77.7b	13.0b	0.7b	89 ab	3.8 ab	38.0a	50.7a	63.2a	1.5bc	85.4a
BT-50	8.5b	64.6a	70.7a	77.6b	13.0b	0.4a	89 ab	4.1 ab	37.7a	50.8a	63.0a	1.2abc	85.4 ab
BT-55	8.6b	68.1b	71.3a	76.3a	8.1a	0.4a	90b	3.7b	38.5a	51.3a	63.1a	0.8a	87.3c
SE	0.1	0.2	0.1	0.1	0.1	0.1	1	0.2	0.4	0.8	0.4	0.2	0.5
Analysis of variance and significance (p-values)													
	**	***	ns	***	***	*	ns	ns	ns	ns	ns	ns	*

ΔH_{gel} = Enthalpy of gelatinization. $T_{O\text{-gel}}$, $T_{P\text{-gel}}$, $T_{C\text{-gel}}$ = Onset, peak and conclusion temperatures of gelatinization. $\Delta T = (T_{C\text{-gel}} - T_{O\text{-gel}})$. $\Delta H_{am\text{-lip}}$ = Enthalpy of the amylose-lipid dissociation. $T_{O\text{-am-lip}}$ = Onset temperature of the amylose-lipid complex dissociation. ΔH_{ret} = Enthalpy of melting of retrograded amylopectin. $T_{O\text{-ret}}$, $T_{P\text{-ret}}$, $T_{E\text{-ret}}$ = Onset, peak and endset temperatures of melting of retrograded amylopectin. $\Delta H_{am\text{-lip-ret}}$ = Enthalpy of the amylose-lipid dissociation at the second scan. $T_{O\text{-am-lip-ret}}$ = Onset temperature of the amylose-lipid complex dissociation at the second scan. ΔH_{gel}, $\Delta H_{am\text{-lip}}$, ΔH_{ret}, $\Delta H_{am\text{-lip-ret}}$ are given in J/g dry matter.
SE: Pooled standard error from ANOVA. Different letters in the same column within each studied variety indicate statistically significant differences between means at $p < 0.05$. Analysis of variance and significance: ***$p < 0.001$. **$p < 0.01$. *$p < 0.05$. ns: not significant.

higher gelatinization temperatures (Li, Li, & Zhu, 2018), so these reduced values could be related to the fragmentation caused to the α-(1, 4) glycosidic bonds, resulting in reduced stability of the crystallites following ultrasonication. The highest treatment temperature caused a greater reduction of T_{C-gel} in BT probably because annealing allowed chain mobility that reduced crystallites stability to an even greater state. The gelatinization enthalpy (ΔH_{gel}) was reduced by the action of cavitation, as can be seen from the results obtained with samples treated at the lowest temperatures, an effect that was counteracted by annealing. Decreased ΔH_{gel} has also been observed in rice starch (Yang et al., 2019) and flour (Vela, Villanueva, Solaesa, & Ronda, 2021) after ultrasonication. Lower values of ΔH_{gel} reflect the degradation of parts of the crystalline regions due to cavitation, especially those containing flaws, and the fragmentation of the linear chains of the amorphous regions that stabilize the crystalline structure (as seen by SEC), thereby facilitating the leaching of amylose out of the granules and water penetration to starch ordered structure, hence reducing the energy required to fully gelatinize the sample (Ding, Luo, & Lin, 2019). Increasing temperatures (≥40 °C for WT samples and ≥50 °C for BT samples) led to significantly equal ΔH_{gel} values than the native samples, believed to be because annealing promotes enhancement of inter- and intra-helical interactions in starches, resulting in an improved arrangement that requires more energy to be melted (Tester, Debon, & Sommerville, 2000). The different temperature where the effect of annealing is seen between ecotypes is related to the different stabilities of the native molecular structures and with the higher gelatinization temperature of the brown ecotype.

Retrogradation transitions were studied with a second scan after 7 days of sample storage at 4 °C. Similar values of ΔH_{ret} were found in ultrasonicated samples of both ecotypes, in agreement with the similar chain fragmentation determined by SEC. This could be because during sample storage at 4 °C, amylose and amylopectin can form double-helical interactions that are lost over the same temperature range as double helices formed exclusively by amylopectin, giving similar results even when their molecular structure has been modified (Klucinec & Thompson, 1999). T_{O-ret} was not modified by sonication, with the exception of WT-50 and WT-55. These results suggest that, even with different molecular structures, the least stable double helices formed during retrogradation in the samples are similar (Li et al., 2020). The enthalpy determined to dissociate the amylose-lipid complex in the second scan ($\Delta H_{am-lip-ret}$) was higher than that of the first scan (ΔH_{am-lip}) in all cases, because of the diffusion of amylose from granules that happens at temperatures above the gelatinization temperature range (Villanueva et al., 2018).

4. Conclusion

The modification achieved by ultrasound treatments were dependent on the tef ecotype, where white tef presented a higher susceptibility. Both ecotypes presented a similar trend with temperature treatment. Cavitation led to physical damage of flour particles' surface and signs of molecular depolymerization in both amylose and amylopectin, with preferential chain fragmentation on the α-(1,4) glycosidic bonds leading to increased proportions of intermediate amylose chains as suggested by SEC results. The narrowing of the gelatinization temperature range indicated that US treatments reduced T_{C-gel} due to disruption of the better packed crystallites, also causing a reduction of ΔH_{gel}. Higher treatment temperatures may have enhanced the mobility and interaction of the amorphous regions within the starch granule that counteracted the effect of US cavitation, leading to a more homogeneous starch configuration after treatments. Amylopectin was affected in a lower degree, without losing the crystalline state in the fragmented chains, resulting in a significant increase of the long-range crystallinity order at treatments performed at higher temperatures. Results indicated that modification of tef flours by US treatments at different temperatures is a feasible technique to change the molecular structure of these GF raw materials and modulate their properties and applicability in GF food

formulations. The alterations obtained in the present study for tef flours could only be partly extrapolated to other matrices. Some of them are very general, resulting from the cavitation phenomenon during low-frequency ultrasound treatments [particle size reduction, breakage of α-(1–4) and/or α-(1–6) linkages], but the degree and extent of the modification, and the molecular structures obtained after the US treatment would greatly depend on the original molecular structure of the studied matrix and its susceptibility to US energy. These structural changes will surely have an impact on the techno-functional properties of the modified tef flours, therefore deeper research on the subject is needed.

CRediT authorship contribution statement

Antonio J. Vela: conceived and designed the experiments; analyzed and interpreted the data, contributed reagents, materials, Formal analysis, tools or data; wrote the paper, performed the experiments, and, wrote the, Writing – original draft, and. **Marina Villanueva:** analyzed and interpreted the data, Writing – review & editing. **Cheng Li:** analyzed and interpreted the data, Writing – review & editing, and. **Bruce Hamaker:** analyzed and interpreted the data, Writing – review & editing. **Felicidad Ronda:** conceived and designed the experiments; analyzed and interpreted the data, contributed reagents, materials, Formal analysis, tools or data; wrote the paper, Funding acquisition, Conceptualization, Methodology, Resources, Investigation, Visualization, Supervision, Writing – review & editing, Project administration.

Declaration of competing interest

Data availability

Data will be made available on request.

Acknowledgement

Appendix A. Supplementary data

Supplementary data to this article can be found online at https://doi.org/10.1016/j.lwt.2023.114463.

References

AACC. (1999). AACC international methods, 44-19.01. Moisture-Air-Oven method. *AACC approved Methods of analysis.* https://doi.org/10.1016/j.beem.2005.04.006.

Abebe, W., Collar, C., & Ronda, F. (2015). Impact of variety type and particle size distribution on starch enzymatic hydrolysis and functional properties of tef flours. *Carbohydrate Polymers, 115*, 260–268. https://doi.org/10.1016/j.carbpol.2014.08.080

Acevedo, B. A., Villanueva, M., Chaves, M. G., Avanza, M. V., & Ronda, F. (2022). Modification of structural and physicochemical properties of cowpea (*Vigna unguiculata*) starch by hydrothermal and ultrasound treatments. *Food Hydrocolloids, 124*, Article 107266. https://doi.org/10.1016/J.FOODHYD.2021.107266

Amini, A. M., Razavi, S. M. A., & Mortazavi, S. A. (2015). Morphological, physicochemical, and viscoelastic properties of sonicated corn starch. *Carbohydrate Polymers, 122*, 282–292. https://doi.org/10.1016/J.CARBPOL.2015.01.020

Babu, A. S., Mohan, R. J., & Parimalavalli, R. (2019). Effect of single and dual-modifications on stability and structural characteristics of foxtail millet starch. *Food Chemistry, 271*, 457–465. https://doi.org/10.1016/J.FOODCHEM.2018.07.197

Bultosa, G. (2016). Teff: Overview. In C. Wrigley, H. Corke, K. Seetharaman, & J. Faubion (Eds.), *Encyclopedia of food grains* (2nd ed., pp. 209–220). Academic Press. https://doi.org/10.1016/B978-0-12-394437-5.00018-8.

Cave, R. A., Seabrook, S. A., Gidley, M. J., & Gilbert, R. G. (2009). Characterization of starch by size-exclusion chromatography: The limitations imposed by shear scission. *Biomacromolecules, 10*(8), 2245–2253. https://doi.org/10.1021/bm900426n

Czechowska-Biskup, R., Rokita, B., Lotfy, S., Ulanski, P., & Rosiak, J. M. (2005). Degradation of chitosan and starch by 360-kHz ultrasound. *Carbohydrate Polymers, 60*(2), 175–184. https://doi.org/10.1016/J.CARBPOL.2004.12.001

Degrois, M., Gallant, D., Baldo, P., & Guilbot, A. (1974). The effects of ultrasound on starch grains. *Ultrasonics, 12*(3), 129–131. https://doi.org/10.1016/0041-624X(74)90070-5

Ding, Y., Luo, F., & Lin, Q. (2019). Insights into the relations between the molecular structures and digestion properties of retrograded starch after ultrasonic treatment. *Food Chemistry, 294*, 248–259. https://doi.org/10.1016/J.FOODCHEM.2019.05.050

Dueñas, M., Sánchez-Acevedo, T., Alcalde-Eon, C., & Escribano-Bailón, M. T. (2021). Effects of different industrial processes on the phenolic composition of white and brown teff (*Eragrostis tef* (Zucc.) Trotter). *Food Chemistry, 335*, Article 127331. https://doi.org/10.1016/J.FOODCHEM.2020.127331

Flores-Silva, P. C., Roldan-Cruz, C. A., Chavez-Esquivel, G., Vernon-Carter, E. J., Bello-Perez, L. A., & Alvarez-Ramirez, J. (2017). *In vitro* digestibility of ultrasound-treated corn starch. *Starch - Stärke, 69*(9–10), Article 1700040. https://doi.org/10.1002/STAR.201700040

Han, X. Z., Campanella, O. H., Mix, N. C., & Hamaker, B. R. (2002). Consequence of starch damage on rheological properties of maize starch pastes. *Cereal Chemistry, 79*(6), 897–901. https://doi.org/10.1094/CCHEM.2002.79.6.897

Karwasra, B. L., Kaur, M., & Gill, B. S. (2020). Impact of ultrasonication on functional and structural properties of Indian wheat (*Triticum aestivum* L.) cultivar starches. *International Journal of Biological Macromolecules, 164*, 1858–1866. https://doi.org/10.1016/J.IJBIOMAC.2020.08.013

Klucinec, J. D., & Thompson, D. B. (1999). Amylose and amylopectin interact in retrogradation of dispersed high-amylose starches. *Cereal Chemistry, 76*(2), 282–291. https://doi.org/10.1094/CCHEM.1999.76.2.282

Li, C., Hu, Y., Huang, T., Gong, B., & Yu, W. W. (2020). A combined action of amylose and amylopectin fine molecular structures in determining the starch pasting and retrogradation property. *International Journal of Biological Macromolecules, 164*, 2717–2725. https://doi.org/10.1016/J.IJBIOMAC.2020.08.123

Li, M., Li, J., & Zhu, C. (2018). Effect of ultrasound pretreatment on enzymolysis and physicochemical properties of corn starch. *International Journal of Biological Macromolecules, 111*, 848–856. https://doi.org/10.1016/J.IJBIOMAC.2017.12.156

Luo, Z., Fu, X., He, X., Luo, F., Gao, Q., & Yu, S. (2008). Effect of ultrasonic treatment on the physicochemical properties of maize starches differing in amylose content. *Starch - Stärke, 60*(11), 646–653. https://doi.org/10.1002/STAR.200800014

Martinez, M. M., Li, C., Okoniewska, M., Mukherjee, I., Vellucci, D., & Hamaker, B. (2018). Slowly digestible starch in fully gelatinized material is structurally driven by molecular size and A and B1 chain lengths. *Carbohydrate Polymers, 197*, 531–539. https://doi.org/10.1016/J.CARBPOL.2018.06.021

Tester, R. F., Debon, S. J. J., & Sommerville, M. D. (2000). Annealing of maize starch. *Carbohydrate Polymers, 42*(3), 287–299. https://doi.org/10.1016/S0144-8617(99)00170-8

Vela, A. J., Villanueva, M., & Ronda, F. (2021). Low-frequency ultrasonication modulates the impact of annealing on physicochemical and functional properties of rice flour. *Food Hydrocolloids, 120*, Article 106933. https://doi.org/10.1016/J.FOODHYD.2021.106933

Vela, A. J., Villanueva, M., Solaesa, Á. G., & Ronda, F. (2021). Impact of high-intensity ultrasound waves on structural, functional, thermal and rheological properties of rice flour and its biopolymers structural features. *Food Hydrocolloids, 113*, Article 106480. https://doi.org/10.1016/J.FOODHYD.2020.106480

Vilaplana, F., & Gilbert, R. G. (2010). Characterization of branched polysaccharides using multiple-detection size separation techniques. *Journal of Separation Science, 33*(22), 3537–3554. https://doi.org/10.1002/JSSC.201000525

Villanueva, M., Abebe, W., Collar, C., & Ronda, F. (2021). Tef [*Eragrostis tef (Zucc.) Trotter*] variety determines viscoelastic and thermal properties of gluten-free dough and bread quality. *Lebensmittel-Wissenschaft und -Technologie, 135*, Article 110065. https://doi.org/10.1016/j.lwt.2020.110065. June 2020.

Villanueva, M., Harasym, J., Muñoz, J. M., & Ronda, F. (2018). Microwave absorption capacity of rice flour. Impact of the radiation on rice flour microstructure, thermal and viscometric properties. *Journal of Food Engineering, 224*, 156–164. https://doi.org/10.1016/j.jfoodeng.2017.12.030

Wang, K., Wambugu, P. W., Zhang, B., Wu, A. C., Henry, R. J., & Gilbert, R. G. (2015). The biosynthesis, structure and gelatinization properties of starches from wild and cultivated African rice species (*Oryza barthii* and *Oryza glaberrima*). *Carbohydrate Polymers, 129*, 92–100. https://doi.org/10.1016/J.CARBPOL.2015.04.035

Wang, L., Wang, M., Zhou, Y., Wu, Y., & Ouyang, J. (2022). Influence of ultrasound and microwave treatments on the structural and thermal properties of normal maize starch and potato starch: A comparative study. *Food Chemistry, 377*, Article 131990. https://doi.org/10.1016/J.FOODCHEM.2021.131990

Wang, M., Wu, Y., Liu, Y., & Ouyang, J. (2020). Effect of ultrasonic and microwave dual-treatment on the physicochemical properties of chestnut starch. *Polymers, 12*(8), 1718. https://doi.org/10.3390/POLYM12081718

Wang, H., Xu, K., Ma, Y., Liang, Y., Zhang, H., & Chen, L. (2020). Impact of ultrasonication on the aggregation structure and physicochemical characteristics of sweet potato starch. *Ultrasonics Sonochemistry, 63*, Article 104868. https://doi.org/10.1016/J.ULTSONCH.2019.104868

Xu, X., Chen, Y., Luo, Z., & Lu, X. (2019). Different variations in structures of A- and B-type starches subjected to microwave treatment and their relationships with digestibility. *Lebensmittel-Wissenschaft und -Technologie, 99*, 179–187. https://doi.org/10.1016/J.LWT.2018.09.072

Yang, W., Kong, X., Zheng, Y., Sun, W., Chen, S., Liu, D., et al. (2019). Controlled ultrasound treatments modify the morphology and physical properties of rice starch rather than the fine structure. *Ultrasonics Sonochemistry, 59*, Article 104709. https://doi.org/10.1016/J.ULTSONCH.2019.104709

Yong, H., Wang, X., Sun, J., Fang, Y., Liu, J., & Jin, C. (2018). Comparison of the structural characterization and physicochemical properties of starches from seven purple sweet potato varieties cultivated in China. *International Journal of Biological Macromolecules, 120*, 1632–1638. https://doi.org/10.1016/J.IJBIOMAC.2018.09.182

Zavareze, E. D. R., & Dias, A. R. G. (2011). Impact of heat-moisture treatment and annealing in starches: A review. *Carbohydrate Polymers, 83*(2), 317–328. https://doi.org/10.1016/J.CARBPOL.2010.08.064

Zhu, F. (2015). Impact of ultrasound on structure, physicochemical properties, modifications, and applications of starch. *Trends in Food Science & Technology, 43*(1), 1–17. https://doi.org/10.1016/J.TIFS.2014.12.008